

Spintronics for electrical measurement of light polarization

H. Dery,* L. Cywiński, and L. J. Sham

Department of Physics, University of California San Diego, La Jolla, California, 92093-0319

(Dated: February 8, 2020)

Abstract

The helicity of a circularly polarized light beam may be determined by the spin direction of photo-excited electrons in a III-V semiconductor. We propose that the electron spin polarization be measured by passing the electrons in parallel through two semiconductor/ferromagnetic metal Schottky barriers with opposite magnetization directions. This proposed detection system would be compact and portable, in contrast with the existing method of light interference in optical cavities.

PACS numbers:

I. INTRODUCTION

The ability to measure the circular polarization of light has greatly facilitated the progress of spintronics research in III-V semiconductor systems¹ in comparison with silicon whose conduction electrons are not optically active. The connection between spin orientation and light polarization in semiconductors is given by the angular momentum conservation rules.² The spin polarization of the electrons in a III-V semiconductor, in the case of a current injection from a ferromagnetic metal, has been measured either by the circular polarization of light from a light emitting diode^{3,4} or by scanning Kerr spectroscopy in a lateral geometry.⁵ The spin polarization has also been measured in the case of extraction current into the ferromagnet by Faraday rotation,⁶ by scanning Kerr spectroscopy,⁵ and by Hanle effect.⁷ The determination of light polarization has, of course, a much broader application in information technology. The current principle of polarimetry is based on the methods of optics, relying on, for example, photoelastic modulators and beam splitter⁸ or the different reflection intensities of polarized light.⁹ The question is whether one can use for polarimetry the reversal of the roles between the ferromagnet/III-V semiconductor and the polarized light. The transmission from the semiconductor to the ferromagnet is spin-dependent¹⁰ and the spin dependence of the photocurrent passing through the junction indicates the sense of the circular polarization of the light exciting the electrons provided the contribution from the magnetic circular dichroism is removed.¹¹

In this paper, we present a scheme to detect the helicity of a circularly polarized light beam as shown in Figure 1. It makes a direct use of the dependence between the magnetization of the contact and the spin polarized electrical current across the semiconductor/ferromagnet tunneling barrier. The beam excites spin-polarized electrons and holes below the stack. The electrons and holes are separated by the p-n junction. The electrons are swept upwards towards the gate and the electrodes. The photocurrent is split through two Schottky barriers with ferromagnets of opposite magnetizations. The different magnitudes of the split currents depend on whether the photo-excited electron spins are parallel or antiparallel to the magnets. The detection scheme takes advantage of the recent advances in the tunnel barrier fabrication either as a Schottky barrier⁴ or separated by an oxide layer¹² which enable efficient transmission of spin currents at room temperature. For the potential practical applications, the monolithic spintronics system is portable and has a much smaller footprint

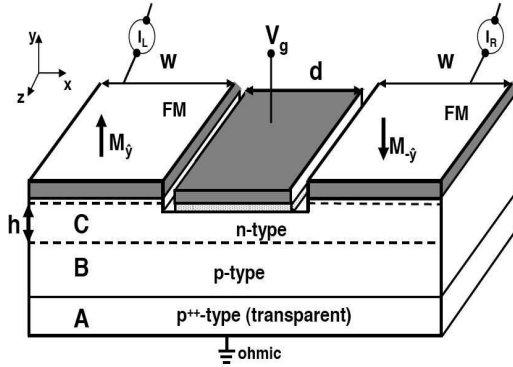


FIG. 1: A scheme of the detector. The conductance of the barriers is controlled by the doping profile beneath the contacts. The metal gate is separated from the channel by a thin insulating barrier.

than the currently available polarimeters. In addition, the phenomenon can be used to detect the amplitude of photo-excited spin accumulation in the semiconductor by a simple electrical measurement. The size of the spin accumulation region may be smaller than the spatial resolution of the scanning magneto-optical techniques (by Faraday or Kerr effects) limited by the wavelength of light.

In the next section we elaborate on important optoelectronics aspects. Section III gives the transport theory of the photo-excited electrons and section IV discusses the results for steady state and pulse operation modes. Conclusions are given in section V.

II. SYSTEM FEATURES

The polarization detection scheme depends on the correlation between the optical and the magnetic properties, which in turn requires the collinearity of the light propagation axis and the ferromagnet magnetization axes. This is simply the conservation of angular momentum when the spin quantization axis lies along the propagation direction of the polarized light. In terms of the axes labeled in Fig. 1, the collinear direction is along the y -axis in which pinning of the magnetization out of plane may be realized by stacking alternate ferromagnetic and antiferromagnetic layers on top of each contact.¹³

The choice of the semiconductor materials is governed by the wavelength of the excitation light. In bulk semiconductors, the upper and lower bounds of the wavelength are set, respectively, by the threshold of band gap transitions and by the onset of transitions between the split-off valence band and the conduction band. For circularly polarized beam

the degeneracy of the heavy and the light hole bands in bulk III-IV compounds leads to our assumption of optical excitation of both types of holes. In order to quantify the spin polarization the beam intensity is decomposed into two generating terms of photo-excited electrons I_+ and I_- which correspond, respectively, to electrons with spin up and spin down. The resulting spin polarization is $\rho \equiv (I_+ - I_-)/(I_+ + I_-) = \pm 1/4$ where the sign depends on the light helicity.²

The gate is essential to the stability of the system. It screens the in-plane electric field due to excess electrons in the channel by bringing “mirror” charges to the metal surface adjacent to the insulator. The screening is effective for a high aspect ratio between the channel length and the thickness of the insulating barrier separating it from the gate. Consequently, the system is electrostatically stable as in MOSFET devices and the transport along the axis connecting the ferromagnets may be assumed to be purely diffusive. The gate may have an additional role if the p-n junction of Fig. 1 is replaced by an alternate design with a unipolar doped structure. In this case the gate should be biased so that a charge accumulation (inversion) layer is formed if an n-doped (p-doped) semiconductor is used. The gate electric field in the semiconductor replaces the built-in field of the p-n junction in the function of sweeping the electrons into the conduction channel. Note that the electron gas in the conduction channel is 3D in the quantum character as we take the effective conduction channel thickness to exceed the electron De-Broglie wavelength.

The scale of the system geometry is set by the spin diffusion length, about 1 μm in GaAs at room temperature, which limits the travel distance of the spin-polarized electrons in the system. For high detection efficiency, the thickness of the conduction channel should be much less than the spin diffusion length. The width of the gate, which attracts the excited electrons to the conduction channel, must also be less than the diffusion length. Below we find the optimal width of each ferromagnetic contact to be less than the spin diffusion length. There is a corresponding important dependence of the efficiency of the lateral semiconductor spin valve on the width of the contacts in the planar geometry.¹⁴ To limit the spins to the active area, the pillar structure is designed to restrict the electrons under the ferromagnetic contacts or between them.

III. ELECTRON TRANSPORT

The polarized beam creates non-equilibrium spin-dependent densities δn_s , $s=\pm$ for spin up or spin down. The resultant spin density, $\delta n_+ - \delta n_-$, gives rise to spin accumulation in the channel. To simplify the following numerical procedures and in order to extract analytical expressions when possible we consider weak excitations. This means that the deviations from equilibrium, δn_s , are one or two orders of magnitude smaller than the free carrier concentration in the paramagnetic channel at equilibrium (n_0). In this regime the electrochemical potential μ_s , may be taken to be linear in δn_s in addition to the electric field term. However the screening action of the gate renders the contribution of this field negligible for transport inside the conduction channel (between the ferromagnets). After excitation, diffusion currents start flowing into the tunneling contacts, equivalent to currents under low forward bias to the Schottky barriers but driven by the spin density gradient, thus,

$$\mathbf{j}_s = \frac{\sigma_s}{e} \nabla \mu_s, \quad (1)$$

where $-e$ is the electron charge and the conductivity in each spin channel is half of the total conductivity of the semiconductor, σ_{sc} . The density profiles are related to the currents by the spin dependent continuity equations,

$$\frac{\partial \delta n_s}{\partial t} = \frac{1}{e} \nabla \mathbf{j}_s - \frac{\delta n_s - \delta n_{-s}}{2\tau_{sp}} + I_s, \quad (2)$$

where $2\tau_{sp}$ is the average flip time between two spin states and I_s is the spin dependent optical generation rate derived from light intensity and absorption coefficient. Combination of the two equations leads to the time-dependent diffusion equation,

$$\frac{1}{D} \frac{\partial \mu_s(x, y)}{\partial t} = \nabla^2 \mu_s(x, y) - \frac{\mu_s(x, y) - \mu_{s-}(x, y)}{2L_{sc}^2} + \frac{2k_B T}{Dn_0} I_s, \quad (3)$$

where D is the semiconductor diffusion constant for the single spin component and $L_{sc} = \sqrt{D\tau_{sp}}$ is the semiconductor spin diffusion length (L_{sc}). The temperature factor comes from our application to the specific case of a non-degenerate semiconductor channel. For the degenerate electrons, it can be easily replaced by the inverse of the derivative of the chemical potential (i.e., the compressibility of the electron gas). We neglect interfacial spin scattering since it is less important than the spin selectivity of the tunneling transmission and, in any case, can be incorporated phenomenologically by the spin-dependence of the barrier conductance.

The boundary condition for the normal component of the spin current across the ferromagnet/semiconductor interface is given by,

$$\sigma_{sc} \left(\hat{n} \cdot \nabla \mu_s \right) = G_s (-eV - \mu_s^i), \quad (4)$$

where \hat{n} denotes the outward interface normal from the semiconductor and G_s is the spin dependent barrier conductance per unit area ($\Omega^{-1}\text{cm}^{-2}$). V is the bias voltage applied to the ferromagnetic contact above this part of the channel. We have replaced the exact description of the electrochemical potential in the ferromagnet with the bias level, justified by the vastly different conductivities of the ferromagnetic metal and the semiconductor ($\sigma_s^{fm} \gg \sigma_{sc}$). In the middle part of the channel the leakage current into the gate is negligible for an insulator layer over 5 nm and so the boundary conditions at the interface are $j_s^y = 0$.

In the conduction channel, the effective spin generation rate, I_s , has a small fraction from direct absorption of light and a major part from photo-excited electrons driven in from the diode region by a strong electric field along the y axis (by the definition of the axes in Fig. 1). In the depleted region, the electric field ($|eE_y| \gg k_B T / L_{sc}$) enhance the downstream spin diffusion length by orders of magnitude.^{15,16} Thus, spin flip processes play negligible role in this region and the carriers flushed across the $y=h$ plane retain their spin orientation. The effective optical generation rate in the channel I_s is thus up-scaled by a factor of $(h+H)/h$, where H is the depletion region width.

The diffusion spin current in the channel is reduced to one dimension.¹⁴ With the axes defined in Fig. 1, the z -dependence is negligible. The two dimensional flow in the channel is reduced to one dimensional along it driven by the vertical (y) average of μ_s

$$\xi_s(x) = \frac{1}{h} \int_0^h dy \mu_s(x, y), \quad (5)$$

where h is the conduction channel thickness, bounded by the gates and the onset of the depletion region for a p - n junction or equivalent for the other mentioned cases. The key two dimensional character retained is the x dependence of the current along the injection contact, a property which is lost in the usual collinear contact/channel/contact one-dimensional model. The present approximation is valid when $h \cdot G_s \ll \sigma_{sc}$, a condition fulfilled in the system under discussion.

We present now the spin current solutions of the effective one-dimensional transport equation under the left and right contacts, occupying, respectively, $x \in [0, w]$ and

$x \in [w+d, 2w+d]$. For a compact form of the solutions, we define inverse diffusion lengths,

$$\begin{aligned}\lambda_{(s,c)}^2 &= [\alpha + 1 \pm \sqrt{1 + \beta^2}] / (2L_{sc}^2), \\ \lambda &= \cot \left[\frac{1}{2} \tan^{-1} \beta \right],\end{aligned}\quad (6)$$

where,

$$(\alpha, \beta) = 2L_{sc}^2(G_+ \pm G_-) / (\sigma_{sc} h_{sc}), \quad (7)$$

where the first of each pair of symbols (s, c) or (α, β) takes the upper sign. In the presence of weak excitation intensities the shape of the tunneling barriers is nearly unaffected. Thus, the antiparallel alignment of the magnetization results with $\alpha_L = \alpha_R$ and $\beta_L = -\beta_R$ where L and R denote, respectively, the left and right tunneling barrier. This symmetry holds if the applied bias is much smaller than the Schottky barrier height (e.g. $|V_L - V_R| < 0.1V$ for Fe/GaAs structures). Also the generation rates are rewritten as

$$I_T = I_+ + I_- \quad I_D = I_+ - I_-. \quad (8)$$

The *steady state* solution beneath the contacts for spatially uniform excitation is given by

$$\begin{aligned}\xi_{\pm}(x) &= (1 \pm \lambda) \left[A e^{\lambda_s x} + B e^{-\lambda_s x} \right] + (\lambda \mp 1) \left[C e^{\lambda_c x} + F e^{-\lambda_c x} \right] \\ &\quad - eV_{L(R)} + \frac{2k_B T L_{sc}^2}{Dn_0} \cdot \frac{(\alpha \mp \beta)(I_T \pm I_D) + 2I_T}{\alpha^2 - \beta^2 + 2\alpha}.\end{aligned}\quad (9)$$

The first line denotes the homogenous solution in which the transport is characterized by two length scales (λ_s^{-1} and λ_c^{-1}). Consider the case that spin polarization is robust so that α and β are comparable. If $\alpha \ll 1$, then $\lambda_c \ll 1/L_{sc}$ and $\lambda_s \sim 1/L_{sc}$. The s -mode is limited by the spin diffusion constant and it corresponds to spin accumulation ($\lambda \gg 1$ in this case). If $\alpha \gg 1$, then both eigenvalues are nearly independent of L_{sc} , and neither of the eigenvectors is a pure spin mode $\lambda \simeq 1$: the inhomogeneity of extraction dominates the spatial dependence. The second line denotes the inhomogeneous solution and is null for zero bias and when excitation is allowed only beneath the gate. In the latter region, the steady state solution is:

$$\begin{aligned}\xi_{\pm}(x) &= A_c + B_c x \pm \left(C_c e^{\frac{x}{L_{sc}}} + F_c e^{-\frac{x}{L_{sc}}} \right) \\ &\quad - \frac{k_B T}{Dn_0} \left(\frac{I_T}{2} x^2 \mp I_D L_{sc}^2 \right).\end{aligned}\quad (10)$$

The term quadratic in x is due to the locally uncompensated charges in the channel, which are neutralized by the gate.¹⁶ The coefficients of the homogeneous solutions are determined by joining ξ_s and its first derivative at the sections of the channel ($x=w$ and $x=w+d$). These conditions correspond to the continuity of densities and currents. In addition, the derivatives vanish at the outer boundaries ($x=0$ and $x=2w+d$). The total current amplitudes in the ferromagnets are:

$$\begin{aligned} I_L &= Z \sum_{s=\pm} \int_0^w \frac{G_s^L}{e} [\xi_s(x) + eV_L] dx \\ I_R &= Z \sum_{s=\pm} \int_{w+d}^{2w+d} \frac{G_s^R}{e} [\xi_s(x) + eV_R] dx \end{aligned} \quad (11)$$

where Z denotes the contact length along the z direction.

IV. RESULTS AND DISCUSSIONS

The key discriminant for the light polarization direction is the current asymmetry (CA) coefficient $= |I_L/I_R - 1|$, where we assume that the currents have been balanced by a small voltage adjustment when the light is unpolarized. We have performed our calculations using the parameters of a GaAs/Fe system at room temperature. The equilibrium electron concentration in the n-type GaAs channel is taken to be $n_0=10^{15}$ cm $^{-3}$ and the effective channel thickness $h=100$ nm. The barrier conductances are $G_+=2G_-=500$ Ω^{-1} cm $^{-2}$ for one contact, and the roles of + and - are switched for the other one. The G_+/G_- ratio and the overall order of magnitude of G_s agree with the polarization and I-V measurements in spin LEDs.¹⁷ In the channel, the semiconductor diffusion coefficient D is 180 cm 2 /sec and the mobility $\nu=7000$ cm 2 /V-sec. The semiconductor spin relaxation time is $\tau_{sp}=80$ ps 2 . Accordingly, the dimensionless quantity $\alpha=2$. We define the barrier's finesse $F\equiv|\beta|/\alpha$, $0\leq F\leq 1$, describing the spin selectivity of the barriers ($F=1$ for the perfect spin injection from a half-metallic ferromagnet). With the reasonable parameters above, $F=1/3$.

Fig. 2a shows the electrochemical potential profiles in the semiconductor channel for excitation level which corresponds to $\delta n_++\delta n_-\simeq 0.04n_0$. The excitation is restricted only to the sub-gate region so that the inhomogeneous term in the second line of Eq. (9) vanishes. The separation of the ferromagnets is $d=200$ nm which is well within the present planar lithography resolution. The contact widths are $3L_{sc}/8=450$ nm. Using these parameters we

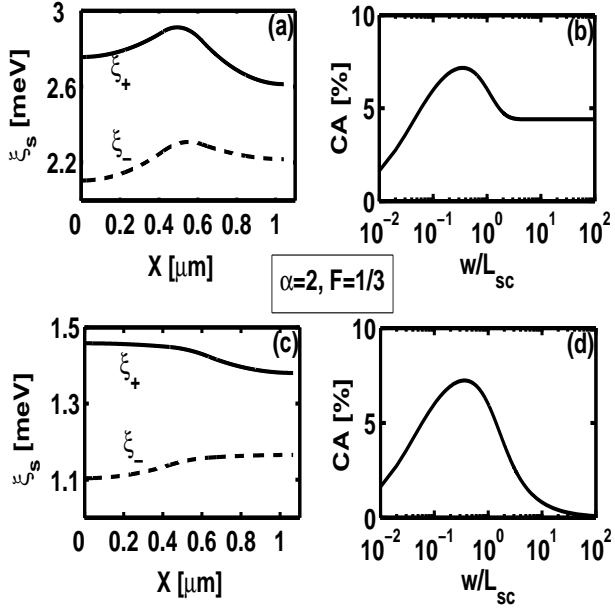


FIG. 2: (a) and (c) show, respectively, the steady state profiles of the electrochemical potentials for excitations restricted only beneath the gate and without such restriction. The spin-up (down) is parallel (antiparallel) to the majority spin axis in the the right ferromagnet. The right current (I_R) is 7% higher than the left current (I_L). (b) and (d) show the respective current asymmetry (CA) coefficient as a function of the ferromagnetic contact width w . For all cases, the temperature is 300K, $V_{fm}^L=V_{fm}^R$ and the same weak intensity level is used. The sub-gate region is centered and extends over 200nm while the rest represents the sub-contact regions. .

obtain a $\sim 7\%$ difference between the left and right ferromagnet currents. We note that the slope of spin-up (spin-down) electrochemical potential is steeper toward the right (left) ferromagnet due to more efficient electrons extraction of this spin. Flipping the helicity results in a mirror image of the spatial profile and in switching roles $\xi_+ \leftrightarrow \xi_-$. The larger current is extracted from the side with the larger spin depletion. Fig. 2b shows the dependence of CA on the ferromagnetic contact width w with an optimal value relative to the spin diffusion length. Figs. 2c and 2d show the respective results where the excitation is allowed beneath the contacts and the gate together. The existence of a peak in the CA may be understood by the behavior in two extreme cases. For contacts whose width exceeds the spin diffusion length the behavior is different for both excitation cases. If the excitation is restricted only beneath the gate region than the asymmetry reaches a finite asymptotic value as the spin

information is already lost when diffuses beyond this width scale. For non-restricted excitation the fraction which contributes to the asymmetry vanishes if $w \gg L_{sc}$ and electrons would tunnel through the barrier under which they were generated. The other extreme of small contacts ($w \ll L_{sc}$) results with similar CA dependence on the contact width as most of the electrons are excited beneath the gate.

The effect of the barrier's conductance (G_s) on CA may be studied directly by varying the doping profile beneath them. The upper panel of Fig. 3 shows the value of CA for optimal value of the contact width as a function of dimensionless parameter α defined in Eq. (7) for three different values of barrier finesse F . In all of the following, the excitation is allowed in all regions. The fixed parameters are the spin diffusion length $L_{sc} = 1 \mu\text{m}$ and the ferromagnets' separation $d = L_{sc}/5$. Curves for different values of ρ and F show that the CA is proportional to ρF and is independent of the excitation level in the linear regime ($|\delta n_{\pm}| \ll n_0$). The linear dependence on the finesse comes from the difference between two currents being linear in the spin selectivity. We recall that in lateral spin valves electrons transverse two barriers leading to quadratic dependence in F . In the detector scheme the role of one ferromagnetic contact (injector) is replaced by the photexcitation process (ρ), and when properly designed the carriers may “select” their preferable extracting terminal.

The optimal contact widths w_{opt} for which these CA values were obtained are plotted in the lower panel of Fig. 3. From the lowering of w_{opt} as α increases, we can infer that CA would decrease for a fixed α as w increases from its optimal value. The lowering of w_{opt} is understood as follows. For highly conductive contacts, the inhomogeneity of extraction dominates the spatial dependence. This means that electrons reaching from the gate region will immediately leave the channel when reaching the contact as it would be the path with minimal resistance. Increasing the contact width allows for spin currents under the far edges but not for charge currents hence diminishing the current asymmetry. Moreover, due to the finite spin dependent conductance and the overall high conductance, photo-excited electrons which are being created beneath the far edge of the contact will rather leave from the same edge leading to further reduction in the asymmetry. This is in contrast to the case of low conductances where the current extraction profile is homogeneous beneath the gates. Finally, we note that w_{opt} is weakly dependent on the finesse of the barriers. This observation simplifies the procedure for choosing the contact width as α can be easily obtained from the I-V curve of the junction without need of the knowledge of β , which is harder to measure.

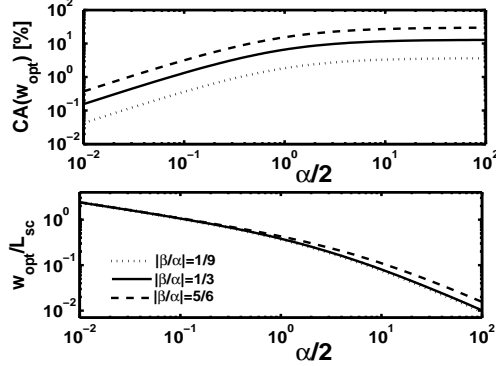


FIG. 3: Upper panel: current asymmetry versus α for three cases of spin selectivity. The calculation is done for the optimal contact width shown in the lower panel. The spin diffusion length is $L_{sc} = 1 \mu\text{m}$ and the separation between the ferromagnetic contacts is $d = 0.2 \mu\text{m}$.

A. Ways to increase the current asymmetry

CA may be improved by increasing the spin diffusion length L_{sc} or by increasing the efficiency of the optically excited spin polarization ρ . The latter may be increased from the bulk value by lifting the degeneracy between heavy and light hole bands by strain or by quantum well confinement.^{2,18,19}

Another alternative is to use higher conductive barriers with narrower contact widths yet within lithography resolution abilities (e.g. $\alpha \simeq 20$ and $w_{opt} \simeq 0.1 L_{sc} \simeq 100\text{nm}$). We note, however, that in the realm of current experiments,^{12,17} acquiring relatively high selectivity is addressed when the ferromagnet/semiconductor interface is abrupt,²⁰ a situation which is achieved with barriers whose α parameter is of the order of unity if non-degenerate semiconductor channels are used. This is not the case in MOSFET devices where the source and drain contacts are alloyed into the semiconductor resulting with a low resistivity but with the expense of a rough interface.²¹ A possible way to overcome the limitation of low α but yet acquiring high finesse is to reduce the Schottky barrier thickness. This could be realized by replacing the silicon dopant at the highly doped interface by tellurium, tin or other dopants.²² For these cases it was measured that self compensation occurred at higher doping levels and that the free carrier concentration was increased by a factor of four. This should halve the thickness of barriers which are presently being used in spin injection experiments, hence leading to an exponential increase in the contact conductance.

Improvement of the spin selectivity ($|\beta| \rightarrow \alpha$), as demonstrated by replacing the Schottky

barrier with an insulating layer¹² of course helps but it was achieved at the expense of a lower α parameter since the conductance of the barrier was very low. This could be improved if a thinner insulator layer is used.

B. Pulse operation

The circular polarization of a pulse of light may also be determined by this spintronics system. We performed a 2D numerical analysis of the time-dependent diffusion equation (3). The initial condition corresponds to a quiescent medium: $\delta n_s(x, t = 0) = 0$. Fig. 4 shows the currents through the two ferromagnetic contacts as a result of excitation by two consecutive Gaussian-shaped pulses of opposite polarization. The width of the pulses is 100 ps. The upper panel denotes a 0.5 GHz repetition rate, with all the parameters as in Fig. 2, where the peak power is an order of magnitude higher than the constant power of the continuous wave used before. The lower panel uses barrier conductances four times larger and 1 GHz repetition rate. The contact widths have been optimized in both cases according to the steady state analysis above. Accordingly, in the higher conductance barriers case (lower panel) the contact widths is $L_{sc}/6$. The contact length along the z axis in Fig. 1 is 1 μm . The rise of the current signals follows the light pulses (not shown), although there is \sim 65 ps (\sim 30 ps) lag between the peak of the light pulse and the peak of the current in the upper (lower) panel. For barriers of lower conductance, the current signal becomes broader due to longer tunneling time of photo-excited carriers through the magnetic contact. In the non-biased system the noise is governed by thermal fluctuations. The pulses of 100 ps amount to a bandwidth of 10 GHz so that the Johnson-Nyquist current is of the order of 10 nA. This value is comparable with the difference between I_R and I_L hence sets an lower bound for the pulse widths. In order to improve the performance one should either improve the CA as discussed previously or use stronger excitations in order to improve the signal to noise ratio.

In order to increase the repetition rate higher conductance barriers are favored so that the current into the ferromagnets is enhanced. Maximal CA is achieved for comparable resistance of the semiconductor layer and of the contacts but for too high conductive barriers the optimal contact width may become impractically small. At the upper panel the time-integrated CA is about 6% whereas the peak to peak ratio is about 9%. In the lower panel

both values are around 11% which is probably due to shorter dwelling time in the channel compared with the pulse width (closer to the steady state solution). We have verified that the time independent solution is recovered for pulses whose duration is much longer than τ_{sp} . The above simulations imply that spin accumulation in short channels could be tracked in time with relatively high repetition rates when the barriers (and/or contact widths) are designed properly.

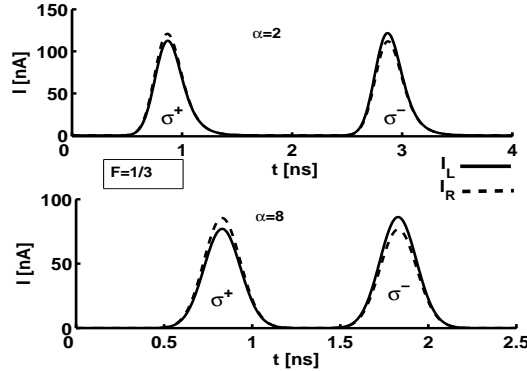


FIG. 4: Time-resolved current response to light pulses alternating in polarization. The solid (dashed) line is from the left (right) magnetic contact. The upper panel denotes lower conductive barriers in which the light pulse rate is 0.5 GHz and the two pulses are centered at 0.8 ns and 2.8 ns. In the lower panel the repetition rate is 1 GHz with two pulses centered at 0.8 ns and 1.8 ns.

V. CONCLUSIONS

We have proposed a spintronics-based scheme for the electrical measurement of circular light polarization. Our analysis provides an aid in choice of system parameters which optimize the detection efficiency. A time-resolved operation is modeled using experimentally verified properties of a Fe/GaAs system with thin Schottky barriers. Room temperature detection is possible in short channels where the current optical detection techniques would be limited by wave length resolution. These features make our scheme easy to integrate and simple to carry out.

This work is supported by NSF under Grant No. DMR-0325599.

* Electronic address: hdery@ucsd.edu

- ¹ S. A. Wolf, D. D. Awschalom, R. A. Buhrman, J. M. Daughton, S. von Molnar, M. L. Roukes, A. Y. Chtchelkanova, and D. M. Treger, *Science* **294**, 1488 (2001).
- ² *Optical Orientation*, edited by F. Meier and B. P. Zakharchenya (Nort-Holland, New York, 1984).
- ³ R. Fiederling, M. Keim, G. Reuscher, W. Ossau, G. Schmidt, A. Waag and L. W. Molenkamp, *Nature* **402**, 787 (1999).
- ⁴ A. T. Hanbicki, B. T. Jonker, G. Itskos, G. Kioseoglou, and A. Petrou, *Appl. Phys. Lett.* **80**, 1240 (2002).
- ⁵ S. A. Crooker, M. Furis, X. Lou, C. Adelmann, D. L. Smith, C. J. Palmström, P. A. Crowell, *Science* **309**, 2191 (2005).
- ⁶ R. J. Epstein, I. Malajovich, R. K. Kawakami, Y. Chye, M. Hanson, P. M. Petroff, A. C. Gossard, and D. D. Awschalom, *Phys. Rev. B* **65**, 121202(R) (2002).
- ⁷ J. Stephens, J. Berezovsky, J. P. McGuire, L. J. Sham, A. C. Gossard, D. D. Awschalom, *Phys. Rev. Lett.* **93**, 097602 (2004).
- ⁸ K.W. Hipps and G.A. Crosby, *J. Phys. Chem* **83**, 555 (1979).
- ⁹ M. S. Ünlü and H. P. Zenginönlü, *Electronics Letters*, **32**, 591 (1996).
- ¹⁰ C. Ciuti, J. P. McGuire and L. J. Sham, *Phys. Rev. Lett.* **89**, 156601 (2002).
- ¹¹ S. J. Steinmuller, C. M. Gürler, G. Wastlbauer and J. A. C. Bland, *Phys. Rev. B* **72**, 045301 (2005).
- ¹² X. Jiang, R. Wang, R. M. Shelby, R. M. Macfarlane, S. R. Bank, J. S. Harris, and S. S. P. Parkin, *Phys. Rev. Lett.* **94**, 056601 (2005).
- ¹³ F. Garcia, J. Moritz, F. Ernult, S. Auffret, B. Rodmacq, B. Dieny, J. Camarero, Y. Pennec, S. Pizzini, and J. Vogel, *IEEE Trans. Magn.*, **38**, 2730 (2002).
- ¹⁴ H. Dery, Ł. Cywiński, and L. J. Sham, *cond-mat/0510770* (2005).
- ¹⁵ Z. G. Yu and M. E. Flatte, *Phys. Rev. B* **66**, 235302 (2002).
- ¹⁶ R. A. Smith, *Semiconductors* (Cambridge University Press, Cambridge, England, 1978).
- ¹⁷ A. T. Hanbicki, O. M. J. van t Erve, R. Magno, G. Kioseoglou, C. H. Li, B. T. Jonker, G.

Itskos, R. Mallory, M. Yasar, and A. Petrou, *Appl. Phys. Lett.* **82**, 4092 (2003).

¹⁸ X. Marie, T. Amand, J. Barrau, P. Renucci, P. Lejeune, and V. K. Kalevich, *Phys. Rev. B* **61**, 11065 (2000).

¹⁹ Y. Ohno, R. Terauchi, T. Adachi, F. Matsukura, and H. Ohno, *Phys. Rev. Lett.* **83**, 4196 (1999).

²⁰ B. T. Jonker, *Proceedings of the IEEE* **91**, 727 (2003).

²¹ S. M. Sze, *Physics of Semiconductor Devices*, (John Wiley, New York, 1981).

²² F. P. Korshunov, N. F. Kurilovich, T. A. Prokhorenko, and V. K. Shesholko, *Inorganic Materials* **38**, 784, (2002).